Neurobiology of Stress 31 (2024) 100660

Contents lists available at ScienceDirect

Neurobiology of Stress

journal homepage: www.elsevier.com/locate/ynstr

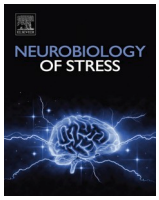

Repeated exposure to multiple concurrent stressors alters visual processing in the adult posterior parietal cortex

Soo Bin Park, Gyorgy Lur *

Department of Neurobiology and Behavior, University of California, Irvine, CA USA, 92697

ARTICLE INFO

Handling Editor: Rita Valentino

Keywords:
Adult stress
Parietal cortex
Visual processing
Individual differences
Longitudinal experimental design

ABSTRACT

Chronic stress is well known to erode cognitive functions. Yet, our understanding of how repeated stress exposure impacts one of the fundamental bases of cognition: sensory processing, remains limited. The posterior parietal cortex (PPC) is a high order visual region, known for its role in visually guided decision making, multimodal integration, attention, and working memory. Here, we used functional measures to determine how repeated exposure to multiple concurrent stressors (RMS) affects sensory processing in the PPC in adult male mice. A longitudinal experimental design, repeatedly surveying the same population of neurons using *in vivo* two-photon imaging, revealed that RMS disrupts the balanced turnover of visually responsive cells in layer 2/3 of the PPC. Across the population, RMS-induced changes in visual responsiveness followed a bimodal distribution suggesting idiosyncratic stress effects. In cells that maintained their responsiveness across recording sessions, we found that stress reduced visual response magnitudes and feature selectivity. While we did not observe stress-induced elimination of excitatory synapses, noise correlation statistics indicated that RMS altered visual input to the neuronal population. The impact of RMS was restricted to visually evoked responses and was not evident in neuronal activity associated with locomotion onset. Together, our results indicate that despite no apparent synaptic reorganization, stress exposure in adulthood can disrupt sensory processing in the PPC, with the effects showing remarkable individual variation.

1. Introduction

Decades of research links repeated or chronic stress exposure to reduced cognitive performance and the development of neuropsychiatric disorders (de Kloet et al., 2005; Bondi et al., 2008; Knauft et al., 2021). One mechanism underlying these negative outcomes is thought to be maladaptive synaptic remodeling and altered connectivity of key brain areas (Liston et al., 2009; Sousa and Almeida, 2012; Radley et al., 2013; Jeanneteau et al., 2018). Best documented are region specific, stress-induced changes in dendritic structure and synapse density in the hippocampus (Woolley et al., 1990; Chen et al., 2008), prefrontal cortex (Radley et al., 2006; Anderson et al., 2016; Jeanneteau et al., 2018), amygdala (Vyas et al., 2002; Mitra et al., 2005; Zhang et al., 2019), and striatal structures (Rodrigues and Monteiro, 2023). Despite indications that chronic stress exposure might alter sensory perception (Girotti et al., 2006; Chen et al., 2018, 2018, 2018; Yochman and Pat-Horenczyk, 2020; Spooner et al., 2021), comparatively little is known about how stress affects sensory processing in the neocortex.

Studies conducted in human subjects suggest that repeated exposure to stress or trauma disrupts the metabolism, function, or connectivity of sensory association regions, like the posterior parietal cortex (PPC) (Bremner et al., 1999; Eckart et al., 2011; Shackman et al., 2011). The PPC is a higher order visual region, often associated with multimodal processing (Whitlock, 2017), attention (Buschman and Miller, 2007), working memory (Suzuki et al., 2022), and decision making (Zhou and Freedman, 2019). Previous work indicates that in adolescent mice, repeated stress exposure disrupts synaptic connectivity of the PPC (Libovner et al., 2020; Fariborzi et al., 2021). However, the impact of prolonged stress exposure during adulthood on parietal function is currently unknown.

Here, we used longitudinal, *in vivo* two-photon imaging to examine how repeated exposure to multiple concurrent stressors (RMS for short) (Chen et al., 2008; Maras et al., 2014; Hokenson et al., 2020) affect sensory responses in the adult PPC. Functional experiments were followed up with immunohistochemistry to test the effect of RMS on excitatory and inhibitory synapses. We found that RMS triggered idiosyncratic changes of visual processing in the PPC.

* Corresponding author.
E-mail address: glur@uci.edu (G. Lur).

https://doi.org/10.1016/j.ynstr.2024.100660
Received 29 March 2024; Received in revised form 25 June 2024; Accepted 29 June 2024
Available online 5 July 2024

2. Materials and method

2.1. Animals

Mice were either purchased from Charles River or bred in house. Adult (8- to 9-week-old) male wild type C57BL/6 mice were group housed on a 12h light/dark cycle with ad libitum access to food and water. All experimental procedures were conducted in accordance with the NIH guidelines on animal welfare and approval by the University of California, Irvine Institutional Animal Care and Use Committee.

2.2. Stress paradigm

Upon reaching postnatal day 60 (±2 days), mice were randomly assigned to either the repeated multiple concurrent stressors (RMS) or control (ctr) group. For stress exposure, mice were placed into the RMS paradigm lasting 4 h per day for ten consecutive days. Mice used for histology experiments were restrained using a well-ventilated 50 ml conical tube whereas mice implanted with titanium head-plates for *in vivo* imaging were restrained in perforated plastic bags. For stress administration, restrained animals were transferred into a clean, transparent cage sitting on a laboratory rocker. In addition to restraint, the stress paradigm consisted of a barrage of sensory stimuli, including recurrent noises (15–30 kHz) played for 0.5–1 s at 0.5–3 s intervals, flashing lights, and rat litter in an unsealed bag (for additional details see Hokenson et al., 2020). Mice in the control group were age matched and handled by the experimenter for the ten RMS days.

2.3. Immunohistochemistry

Following ten consecutive days of RMS, mice were sacrificed and their brains processed for immunohistochemistry as previously described (Libovner et al., 2020; Fariborzi et al., 2021). Briefly, mice were transcardially perfused with phosphate buffered saline (PBS) followed by 4% paraformaldehyde (PFA) in PBS. After 6 h of post-fixation in 4% PFA, 50 μm coronal sections containing the posterior parietal cortex (PPC) were prepared using a vibrating microtome (Compresstome 300z). Non-specific antibody binding was blocked using 10% normal goat serum (NGS, SIGMA), 1% bovine serum albumin (BSA, SIGMA), and 0.1% Triton (SIGMA) in Sorenson's buffer for an hour at room temperature. Sections were then transferred into staining solution containing 5% NGS, 1% BSA, and the primary antibody against postsynaptic density 95 (PSD95, #7E3-1B8, ThermoFisher, 1:2000 dilution), Gephyrin (#147 021, Synaptic Systems, 1:2000 dilution), or cFos (#226-003, Synaptic Systems, 1:5000 dilution) in Sorenson's buffer overnight at 4 °C. The next morning, slices were washed in Sorenson's buffer prior to the addition of a secondary antibody conjugated to AlexaFluor488 (1:1000) or AlexaFluor555 (1:500, ThermoFisher) and the deep-red Nissl stain NeuroTrace640 (1:50 dilution, Thermo Fisher Scientific) in Sorenson's buffer for 2 h at room temperature. Slices were then mounted onto microscope slides with Prolong Diamond anti-fade medium.

2.4. Confocal microscopy

Confocal images of immunostained tissue were collected on a LSM700 Confocal Microscope (Zeiss) located in the University of California, Irvine Optical Biology Core. The PPC was identified as described previously (Libovner et al., 2020; Fariborzi et al., 2021), and a full column of the posterior parietal cortex was tiled (3x10) at 1x zoom (0.2 μm pixel size) using a 63× oil-immersion objective. Fluorescence was excited via 488 nm, 561 nm, or 640 nm laser lines and emissions were directed into PMT through a beam splitter and filtered for minimal spectral overlap: 410–604 nm for AlexaFluor488, 490–560 nm for Alexafluor555, and 643–700 nm for Neurotrace640.

2.5. Image quantification

To quantify synapse density, a 100 μm^2 area was randomly selected form each layer of the PPC column. Synaptic puncta were counted using unbiased, automated batch processing in CellProfiler (Lamprecht et al., 2007), as described in (Libovner et al., 2020; Fariborzi et al., 2021). Synapse densities were expressed as the number of puncta per 100 μm^2. To quantify cFos expression, NeuroTrace and cFOS positive cells were counted in CellProfiler as previously described (Libovner et al., 2020). The NeuroTrace signal established total neuron count. cFos expression was given as the proportion of cells showing colocalization of cFos and NeuroTrace over the total number of neurons detected in the image. Immunostaining data was collected from 2 to 3 PPC sections from each animal, the resulting synapse or cell counts were then averaged, and statistical comparisons were made on a per animal basis.

2.6. Surgical procedures

For *in-vivo* imaging experiments, we expressed the genetically encoded calcium indicator, GCaMP6s, under the hSynapsin promoter via transcranial injection of an adeno-associated viral vector (AAV2.1-hSynapsin-GCaMP6s, Addgene) as previously described (Lur et al., 2016). Briefly, mice (postnatal day 30 ± 2) were deeply anesthetized and the right PPC (AP: 2.0, ML: 1.7, DV: 0.35 from Bregma) was targeted via a stereotaxic apparatus (KOPF Instruments). The viral vector (300 nL) was injected through a glass capillary using a standard microinjection pump (UMP3, World Precision Instruments). Following two weeks of recovery, under deep anesthesia, the scalp was removed and a custom titanium headplate was secured to the skull using dental cement (Metabond). A circular craniotomy was made centered on the right PPC using a high-speed handheld drill and a dual-glass cranial window (a 3 mm cover slip bonded to a 5 mm cover slip using an UV curing adhesive (Norland Products)) was secured to the skull. Mice were allowed two weeks to recover and habituate to the microscope prior to imaging.

2.7. In-vivo imaging

Mice expressing GCaMP6s in the PPC were first habituated to the running disk in a custom built-rig created for awake, head-fixed measurements (Ozgur et al., 2023). The apparatus was situated under a two-photon laser-scanning microscope (MOM, Sutter Instruments). Excitation through a 20×, water immersion objective (0.95 NA, Olympus) was driven by a Ti-Sapphire pulsed laser (Chameleon Ultra 2, Coherent) tuned to 940 nm. Images (256 x 256 pixels) were acquired using the ScanImage 5.4 software (Vidrio Technologies) at 30Hz frame rate from cortical layers II/III (150-250μm depth relative to the cortical surface). The timing of each frame was recorded using a data acquisition board (National Instruments) at 5 kHz via WaveSurfer (Adam L. Taylor, Janelia Research Campus (https://wavesurfer.janelia.org)). Fluorescence emissions were filtered at 525/70 nm bandpass and collected via a GaAsP PMT (Hammamatsu). Imaging was conducted pre-stress (p60 ± 2) and repeated following 10 days of rest or RMS in all animals. Cortical location was recorded by imaging the blood vessel patterns at the brain surface and the field of view across the two imaging days was matched using the built-in motion correction function of ScanImage.

2.8. Visual stimulus

Stimuli were driven via a custom, MATLAB-based graphical user inface (Ozgur et al., 2023). An LED panel (16x9 pixels) was placed in front of the animal's left eye at approximately 45 degrees to the animal's axis. Blinking (5Hz, 50% duty cycle) stationary bars (2-pixel width) at either 45, 90, 135, or 180 degrees orientation were displayed for 1 s with an intertrial interval randomly drawn from a distribution of 9–12s. The timing of the stimulus was recorded simultaneously with the microscope frames using a data acquisition board (National Instruments) at 5 kHz

via WaveSurfer.

2.9. Quantifying locomotion

We measured the locomotion of all animals throughout the imaging sessions via a rotary encoder on the running disk (see detailed description here: https://github.com/LurLab-UCI/RunDisc). The output of the encoder was recorded simultaneously with the microscope frames and stimulus presentations using a data acquisition board (National Instruments) at 5 kHz via WaveSurfer. Rotary encoder signals were processed through custom MATALB script (https://github.com/LurLab-UCI/RunDisc/wiki/decode-rotation). We characterized locomotion based on speed, with at least 2 s between running bouts, and running duration of at least 3 s; the signal was filtered for jitter on the wheel using a low pass filter of 0.25Hz (Niell and Stryker, 2010; Vinck et al., 2015). Only mice with a minimum of six locomotion bouts per session (for both experimental time-points) were included in locomotion analyses.

2.10. Calcium imaging data analysis

Longitudinal calcium imaging data was registered and segmented using Suite2P (Pachitariu et al., 2016). The two imaging sessions (pre- and post- RMS/rest) were processed together and manually curated to track matching cells within the field of view. Cells that were not matched across the two sessions were excluded. All further analyses were performed using custom Python 3.9 (Anaconda distribution) scripts. After subtracting the neuropil signal, fluorescence intensity traces extracted from every identified cell were aligned to stimulus onset using the recorded microscope frame signal. Calcium signals were normalized as:

$$F_{norm} = \frac{\Delta F}{F_0},$$

with F_0 defined as the mean fluorescence 2s prior to stimulus onset. Rarely, fluorescence intensity traces showed fluctuations greater than two standard deviations from the mean, such traces were omitted from analysis. Calcium transients were averaged across all trials of the same stimulus orientation, and the area under the curve from stimulus onset to the subsequent 3 s was calculated to measure the response magnitudes. Cells were classified visually responsive if stimulus presentation caused the calcium trace to deviate from baseline, quantified as a significant difference (mixed-effects model, $p < 0.05$) between the pre- and post-stimulus onset slopes (slope coefficient of a linear regression model fitted to last 1.5s of the baseline vs. first 1.5s after stimulus onset). The same process was used to detect cells responsive to locomotion onset. Animals that either ran throughout or remained still for the entire recording session were excluded from locomotion analysis.

Response magnitudes were calculated as the area under the first 3 s of the evoked calcium transient, starting at stimulus (or locomotion) onset. Of the four visual stimuli, the one with the largest absolute response magnitude was considered the preferred orientation. The presentation of only 4 oriented stimuli, and the presence of negative (suppressed) responses was not conducive to classical analyses of orientation tuning. Thus, to measure the effect of RMS on feature selectivity, we approximated orientation tuning width with the variance of response magnitudes across stimuli compared to the preferred orientation:

$$S^2_{2,3,4} = \frac{\sum (x_i - \overline{x}_{PO})^2}{n-1},$$

where x_{PO} was the response to the preferred orientation and x_i the response to each of the other stimuli. To estimate the effect of RMS on response consistency, we calculated the variance in the response magnitudes across repeated presentations of the preferred orientation. Two neurons, that showed activity three standard deviations away from the mean of all stably responsive cells, were removed from these analyses.

To determine how PPC neurons altered their response to visual stimulus across the two recording sessions, we labeled cells as "lost" if they were only responsive during the first, pre-stress/rest recording, and labeled them as "gained" if they were only responsive during the second, post-stress/rest session. We termed cells that were visually responsive in both sessions "stable". The proportion of cells that changed their behavior was calculated as:

$$\frac{\text{number of cells}_{\text{GAINED}} + \text{number of cells}_{\text{LOST}}}{\text{total number of recorded cells in session 2}}.$$

To determine whether the in each animal the gain and loss of responsive cells was in balance we calculated a G/L balance index:

$$abs\left(\frac{\text{number of cells}_{\text{GAINED}} - \text{number of cells}_{\text{LOST}}}{\text{number of cells}_{\text{GAINED}} + \text{number of cells}_{\text{LOST}}}\right),$$

where values close to 0 indicate that the number of gained and lost cells were similar, whereas higher values indicate that the distribution is skewed towards greater amount of change, regardless of direction.

To quantify the amount of change in the number responsive cells per mouse, we took the following ratio:

$$\frac{\text{number of responsive cells}_{\text{post}}}{\text{number of responsive cells}_{\text{pre}}}.$$

We visualized this distribution using kernel density estimation plot and applied Levene's test to assess homogeneity of variance between the control and stress groups. To assess normality while accounting for skew and kurtosis, we utilized the D'Agonstino-Pearson test. Unimodality was tested using Hartigan's dip test (Hartigan and Hartigan, 1985) after bootstrapping ($n = 100$) to better simulate population patterns.

To estimate the strength of common visual input to PPC neurons we performed noise correlation analyses (Cohen and Kohn, 2011) as previously described (Lur et al., 2016). Using custom Matlab scripts, we calculated the pair-wise correlation in trial-by-trial response magnitude fluctuations across all cells in each field of view. To remove the influence of common network fluctuations (e.g. state transitions) we computed partial correlation coefficients and expressed the correlation of the neuronal population as the average across all cells.

2.11. Statistics

Statistical comparisons of synapse density (PSD95 and Gephyrin) used one-way ANOVA, followed by Sidak's correction for multiple comparisons. To compare cFos expression across control and stress conditions at different timepoints, we ran a two-way ANOVA with a Sidak's post-hoc test. In all immunostaining experiments, individual animals were treated as independent observations, within animal data were averaged.

For the calcium imaging data that did not meet the assumptions for parametric testing, we used non-parametric statistical models. Specifically, we used Mann Whitney test for unpaired comparisons between control and RMS groups and Wilcoxon rank-sum test for paired measurements. To assess distribution patterns, we tested for normality using D'Agostino and Pearson test. For datasets that did not have a normal distribution, we followed up with a test for unimodality, utilizing Hartigan's Dip Test. All response magnitude comparisons for stably responsive cells were calculated using paired statistics (Wilcoxon-rank-sum test). The percentage of cells per mouse that changed their preferred orientation across the two timepoints (Supplementary Fig. 2) were compared using the Mann Whitney test.

All statistical comparisons were executed in Prism version 9 (GraphPad), with the exception of tests assessing homogenous variance using Levene's test and Hartigan's dip test, which were executed using open-source packages in Python. Noise correlation data across stress

condition and session timing (pre. vs. post) were compared using two-way ANOVA, with Fisher's LSD test to compare subgroups.

3. Results

3.1. RMS induced idiosyncratic changes in visual responsiveness of layer 2/3 PPC neurons

We employed a longitudinal strategy to determine the impact of repeated exposure to multiple concurrent stressors (RMS) on sensory processing in the PPC of young adult mice. We recorded responses of GCaMP6s expressing layer 2/3 neurons to passively viewed visual stimuli using two-photon calcium imaging in awake, head-fixed mice on the day prior to RMS and on the day following the final stress session. By matching the field of view before and after RMS, we tracked the activity of the same neurons across the two timepoints (Fig. 1A). Age matched control animals were subjected to identical experimental conditions without RMS exposure. Based on visual responsiveness, we characterized PPC neurons into four categories: non-responsive, gained (non-responsive pre- but responsive post-treatment), lost (responsive pre- but non-responsive post-treatment), or stable (responsive at both timepoints) (Fig. 1B). We further characterized responsive cells as enhanced (RE) or suppressed (RS) based on the stimulus inducing a positive or negative deflection from baseline, respectively. We found no change in the overall proportion of visually responsive PPC neurons in either control or RMS exposed mice ($F_{(1,20)}$, 0.391, $p = 0.539$, $n_{ctr} = 11$, $n_{RMS} = 11$, two-way repeated measures ANOVA, Fig. 1C). Neither did RMS impact the overall proportion of cells that changed their behavior across the sessions ($p = 0.44$, $n_{ctr} = 11$, $n_{RMS} = 11$, unpaired *t*-test). However, we found that RMS altered the balance of gained and lost responsive cells (Mann-Whitney $U = 27$, $p = 0.028$, Mann Whitney test, Fig. 1D). This suggested that population means, may obscure nuanced changes in sensory responsiveness.

To represent the rate of change in the fraction of visually responsive neurons in individual mice (see population data in Supplementary Fig. 1A), we took the ratio of the number of responsive cells in the first and second imaging session (Fig. 1E). We found a significant increase in variance across RMS mice, with the absolute difference from a ratio of 1 markedly larger in RMS ($p = 0.003$, Levene's test, Fig. 1E). These data indicated a highly heterogeneous response to stress exposure. To further explore this phenomenon, we used bootstrapping to produce a more representative sample of the control and RMS populations, and found a significant deviation from normality in RMS, but not in control samples ($K^2_{RMS} = 51.90$, $p < 0.0001$; $K^2_{ctr} = 5.389$, $p > 0.05$, d'Agostino-Pearson test). Hartigan's dip test revealed that the RMS population is bimodally split between mice that gained (G) or lost (L) visually responsive cells ($p < 0.0001$, Hartigan's dip-test). To examine what drove the increased variance in the RMS group, we compared the magnitude of enhanced and suppressed responses across mice that showed a net gain or a net loss of responsive neurons (Fig. 1F). We found that the response magnitude of enhanced cells increased from the pre-to the post-RMS session in mice that gained visually responsive cells, but decreased in mice that lost responsive neurons ($F_{(1,9)} = 9.655$, $interaction_{session\ x\ type}$ $p = 0.013$, $n_{gained} = 5$, $n_{lost} = 6$, two-way repeated measures ANOVA). Response amplitudes of suppressed neurons followed a similar pattern: showing larger post-RMS responses in mice that gained responsive cells but reduced responses in those that lost cells ($F_{(1,9)} = 6.007$, $interaction_{session\ x\ type}$ $p = 0.037$, $n_{gained} = 5$, $n_{lost} = 6$, two-way repeated measures ANOVA).

Overall, we found that RMS exposure threw the turnover of visually responsive neurons in the PPC out of balance. The directionality of this change showed a bimodal split in the stress-exposed population, with some mice gaining, while others losing responsive neurons. Which category a mouse belonged to was consistent with the overall change in the magnitude of visual responses, suggesting individual differences in adaptation strategies.

3.2. RMS altered visually evoked responses of excited neurons

To gain a more direct insight into how RMS affected sensory responses of individual cells, we focused on the neuronal population that showed responsiveness in both imaging sessions (stable cells). We expressed the absolute RMS-induced change in visually evoked responses as a ratio of post-over pre-treatment response magnitudes for sign-conserved (consistently enhanced or suppressed) cells. On average, we found no change in control mice, while RMS exposure reduced the response magnitude of stable cells by approximately 13% ($median_{ctr} = 0.918$, $median_{RMS} = 0.786$; Mann-Whitney $U = 34351$, $p = 0.017$, $n_{ctr} = 305$, $n_{RMS} = 255$, Mann Whitney test, Fig. 2A).

To gauge what was driving this reduction, we compared pre- and post-treatment responses separately for enhanced and suppressed neurons. In control animals, response magnitudes of stable cells remained unaffected across the two imaging sessions (RE_{ctr} $p = 0.108$, $n = 217$; RS_{ctr} $p = 0.774$, $n = 88$, Wilcoxon signed rank test, Fig. 2B), consistent with the unchanged ratio above. In contrast, RMS reduced the response magnitude of neurons that showed an enhanced response to visual stimuli, but not of those cells that were suppressed (RE_{RMS} $p < 0.0001$, $n = 140$; RS_{RMS} $p = 0.721$, $n = 115$, Wilcoxon signed rank test, Fig. 2B). Mean response traces for the entire population are shown in Fig. 2C. These results suggest that the net excitatory drive to visually responsive pyramidal cells in the PPC was reduced following 10 days of RMS exposure.

To ask how RMS affected visual feature selectivity in stable cells, we approximated orientation tuning width by calculating the variance in response magnitudes across the four orientations (see Methods). Using this relatively crude metric, a more broadly tuned cell would show less variance across stimuli, i.e. more similarity to the preferred orientation (see example polar plots in Fig. 2D). We found that the variance across orientations was more substantially reduced in PPC neurons of RMS exposed animals than in controls (Mann-Whitney $U = 33144$, $p = 0.004$, $n_{ctr} = 304$, $n_{RMS} = 254$, Mann Whitney test, Fig. 2E). We also found that a very large proportion of PPC neurons changed their orientation preference between the two time points, with no effect of RMS (ctr: 73.7%, RMS: 75% of cells changing their orientation preference, Mann-Whitney $U = 49$, $p = 0.47$, $n_{ctr} = 11$, $n_{RMS} = 11$ mice, Mann Whitney test, Supplementary Fig. 2).

In a prior study, stress exposure induced considerable within subject heterogeneity in neural activity patterns (Barthas et al., 2020). To test the effect of RMS on the consistency of visual responses, we measured the variance in response magnitude across the repeated presentations of the preferred orientation in stably responsive neurons. We found that in controls, response variance remained unchanged (median post/pre ratio = 1.011, $p = 0.17$, $n = 304$, Wilcoxon signed rank test, Fig. 2F top). Surprisingly, in RMS exposed mice, stress exposure led to a decrease in response variance (median post/pre ratio = 0.833, $p < 0.0001$, $n = 254$, Wilcoxon signed rank test, Fig. 2F bottom), showing a marked difference than the controls (Mann-Whitney $U = 30095$, $p < 0.0001$, Mann Whitney test, Fig. 2G).

3.3. Locomotion responses were not impacted by RMS

Activity of cortical neurons, including those in the visual system, is well known to be modulated by arousal and locomotion (Niell and Stryker, 2010; Vinck et al., 2015). Given the mechanistic role of potentially stress-sensitive neuromodulator systems in arousal processes (Polack et al., 2013; Fu et al., 2014; Collins et al., 2023), we wanted to test the effect of RMS exposure on PPC neuronal responses to locomotion onset.

First, we measured the proportion of locomotion responsive cells (LRCs) per mouse, separating cells into gained, lost, or stable, enhanced or suppressed categories. We found no RMS induced differences in PPC neuronal responses to locomotion onset ($interaction_{time\ x\ condition}$ $F_{(1,17)} = 0.382$, $p = 0.544$; main $effect_{time}$ $F_{(1,17)} = 4.621$, $p = 0.046$; $n_{ctr} = 9$,

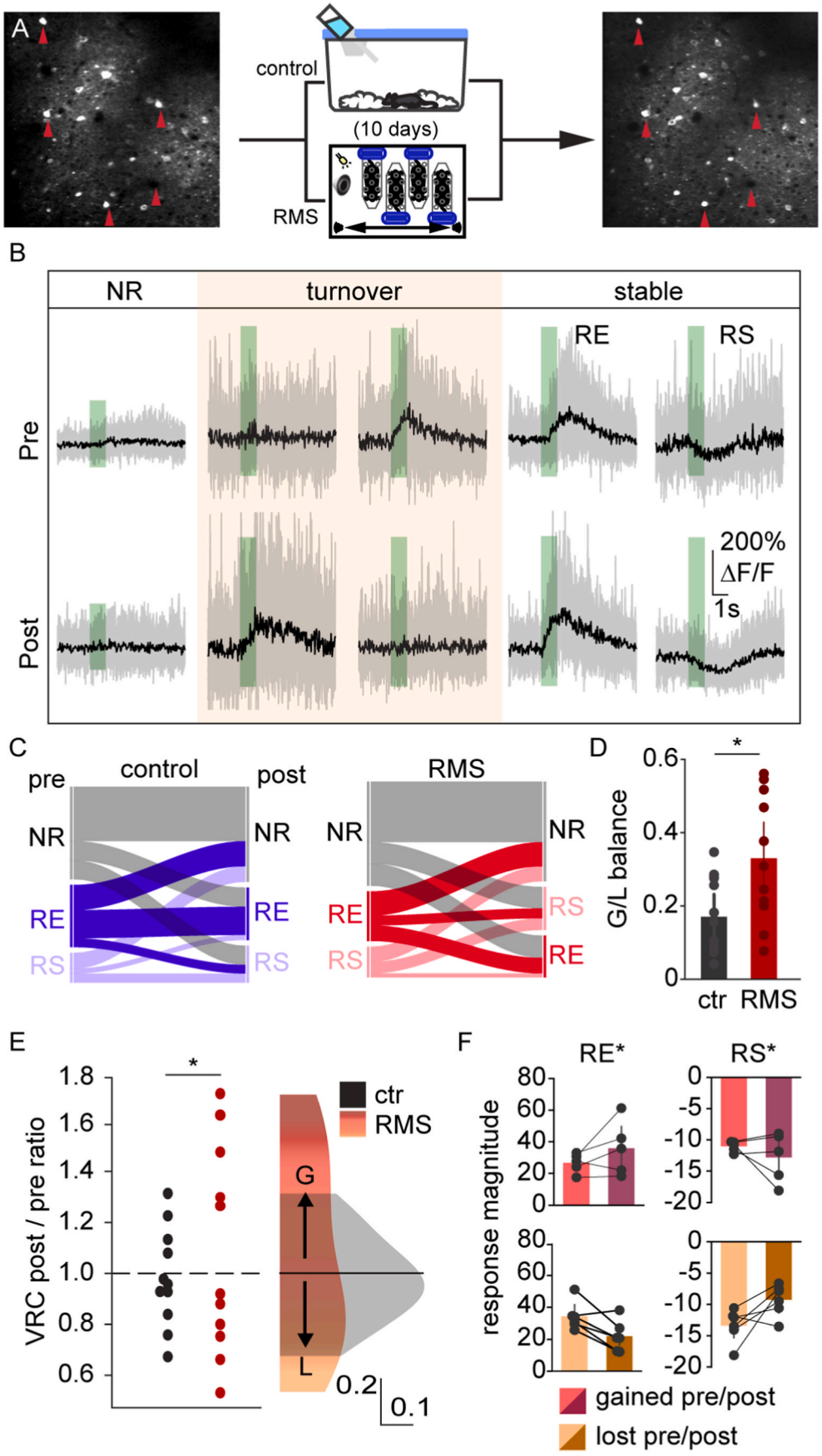

(caption on next page)

Fig. 1. RMS altered the balance of visually responsive neuron turnover in the PPC. (**A**) Experiment schematic showing a representative field of view in the first recording session (left), followed by 10 days of RMS or rest (middle), and a second imaging session from the same field of view (right). (**B**) Representative fluorescence intensity traces from non-responsive cells (NR), cells that alter their responses across sessions (turnover) and cells with stable responses (stable) showing example neurons with enhanced (RE) and suppressed (RS) response characteristics. Light grey traces are individual trials, black traces are mean across the session, green box indicates stimulus presentation. (**C**) Sankey plots showing pooled population dynamics. Line thickness represents the relative proportion within the population. (**D**) Bars represent the G/L balance index in control (dark grey) and RMS (red) mice. (**E**) Ratio of visually responsive cells (VRCs) across the two recording sessions (left) in control (black) and RMS (red) mice plotted next to corresponding kernel density estimation (right). Scale bar shows the ratio vs. density. (**F**) Mean response magnitudes of enhanced and suppressed response type neurons separated by individual animals falling on opposite sides of the binomial distribution in (E). *: $p < 0.05$. Error bars represent 95% CI. (For interpretation of the references to color in this figure legend, the reader is referred to the Web version of this article.)

$n_{RMS} = 10$, two-way repeated measures ANOVA, Fig. 3A). We calculated G/L balance index for LRCs similarly to visually responsive neurons and found no difference in responsive cell turnover between control and stressed groups (Mann-Whitney $U = 42$, $p = 0.842$, $n_{ctr} = 9$, $n_{RMS} = 10$, Mann Whitney test, Fig. 4B). Calculating the ratio of locomotion responsive neurons across the two imaging sessions (see population data in Supplementary Fig. 1B) revealed that the rate of change was indistinguishable between control and RMS animals (Mann-Whitney $U = 37.5$, $p = 0.563$, $n_{ctr} = 9$, $n_{RMS} = 10$, Mann Whitney test, Fig. 3C). Accordingly, we found similar variance across mice in the two groups ($p = 0.437$, Levene's test) with indistinguishable distributions following bootstrapping ($K^2_{RMS} = 5.545$, $p > 0.05$; $K^2_{ctr} = 4.081$, $p > 0.05$, D'Agostino-Pearson).

To quantify the effect of RMS on locomotion response magnitudes, we again focused on stable cells (neurons with detectable responses in both sessions). There was no measurable difference in the ratio of post- over pre-treatment response magnitudes between control and RMS groups ($median_{ctr} = 0.975$, $median_{RMS} = 0.835$; Mann-Whitney $U = 3970$, $p = 0.431$, $n_{ctr} = 99$, $n_{RMS} = 86$, Mann Whitney test, Fig. 3D). However, no difference in ratios may be driven by opposing effects on enhanced and suppressed response exhibiting neurons. Thus, we split cells according to their response type, but found no change in the response magnitudes of either group (RE_{ctr} $p = 0.921$, $n = 93$; RE_{RMS} $p = 0.164$, $n = 78$; RS_{ctr} $p = 0.688$, $n = 6$; RS_{RMS} $p = 0.313$, $n = 8$, Wilcoxon signed ranks test, Fig. 3E). Average traces across all stable cells are shown in Fig. 3F. These data indicate that locomotion responses of L2/3 PPC neurons remained unaffected by RMS exposure.

3.4. RMS did not impact PPC synapse density in adults

A single exposure to multiple concurrent stressors in adult mice has been shown to cause significant loss of dendritic spines from the dorsal hippocampus (Chen et al., 2008, 2010; Maras et al., 2014; Hokenson et al., 2021). We hypothesized that synapse loss may explain the RMS-induced change in visual processing in the adult PPC as well. To quantify synapses, we visualized excitatory and inhibitory post-synaptic proteins (PSD95 and Gephyrin) in the PPC using indirect immunostaining (Fig. 4A). However, we found no significant differences in the density of PSD95 (Fig. 4B) or Gephyrin (Fig. 4C) puncta between RMS and control groups (PSD95: $F_{(7,111)} = 3.156$, $p = 0.004$, one-way ANOVA; $p_{L1} = 0.994$, $p_{L2/3} = 0.959$, $p_{L5} = 0.950$, $p_{L6} = 0.998$, $n_{ctr} = 14$, $n_{RMS} = 12$, corrected for multiple comparisons using Sidak's test; Gephyrin: $F_{(7,71)} = 9.536$, $p < 0.0001$, one-way ANOVA; $p_{L1} = 0.994$, $p_{L2/3} = 0.999$, $p_{L5} = 0.999$, $p_{L6} = 0.695$, $n_{ctr} = 12$, $n_{RMS} = 7$, Sidak's test). These results indicate that in the PPC, exposure to RMS during adulthood did not impact synapse densities on average.

The above finding was in stark contrast to previous work that found significant, persistent, and layer-specific synapse loss in the PPC when mice were exposed to RMS during adolescence (Libovner et al., 2020; Fariborzi et al., 2021). A possible explanation of this discrepancy would be greater extent of habituation to repeated stress exposure in adults (Grissom and Bhatnagar, 2009). To test this, in a separate cohort of mice we stained for cFos (Fig. 4D), an immediate early gene often associated with stress-induced activation of neurons (Lkhagvasuren et al., 2014). Following the first bout of RMS, we found a large proportion of $cFos^+$ cells in the PPC, which returned to control levels by the tenth, final session (Fig. 4E). Comparing control and RMS mice revealed a significant interaction between stress condition and exposure time ($F_{(1,16)} = 6.96$, $p_{treatment\ x\ time} = 0.018$, $n_{ctr\ D1,\ D10} = 5, 4$, $n_{RMS\ D1,\ D10} = 6, 5$, two-way ANOVA). Indeed, post-hoc analysis only showed a statistically significant effect of exposure time in the RMS mice ($p_{ctr} = 0.415$, $p_{RMS} = 0.041$, Sidak's test). This suggests that unlike in adolescent mice, the initial effect of RMS on parietal neurons was attenuated in adults as the animals repeatedly experienced the same stressors over ten days.

3.5. RMS reduced visually evoked network correlations

Finally, we wanted to determine how RMS exposure in adulthood impacts the correlation structure of the PPC network. Such measures would allow us to estimate changes in synaptic connectivity or common input to local neurons (Schneidman et al., 2006; Cohen and Kohn, 2011). To this end, we computed pair-wise noise correlations between all recorded cells in pre- and post-treatment imaging sessions (Fig. 5A). We found that in control animals, average correlation strength increased from the first to the second session ($p_{ctr} = 0.031$, $n = 10$, Fischer's LSD post-hoc test) but such a change was not detected in RMS exposed animals ($p_{RMS} = 0.347$, $n = 10$, Fischer's LSD post-hoc test). Two-way ANOVA indicated an interaction effect between the elapsed time and stress exposure ($F_{(1,18)} = 5.470$, $p_{interaction} = 0.03$, Fig. 5B). In contrast, we found no difference in the correlation structure of control and RMS animals when analyzing locomotion responses ($F_{(1,16)} = 1.215$, $p_{interaction} = 0.287$, $n_{ctr} = 10$, $n_{RMS} = 10$, two-way ANOVA, post-hoc Fischer's LSD $p_{ctr} = 0.835$, $p_{RMS} = 0.197$, Fig. 5C). These results suggest that RMS selectively impacted the visual input received by PPC L2/3 neurons.

4. Discussion

In the current study we show that in adult male mice, repeated exposure to multiple concurrent stressors (RMS) alters visual processing in the posterior parietal cortex (PPC). Longitudinal recordings of matched sets of neurons revealed that RMS disrupts the balanced turnover of visually responsive cells in layer 2/3 of the PPC. Across the population, changes in visual responsiveness followed a bimodal distribution suggesting idiosyncratic stress effects across mice. In cells stably responsive across recording sessions, we found reduced visual response magnitudes and broadened tuning. Noise correlation analyses indicated that stress altered common visual input to parietal neurons. In contrast, locomotion responses remained unchanged by RMS exposure, indicating that the effects may be specific to sensory circuits. Surprisingly, the above findings were not coupled with wide-spread RMS-induced synapse loss.

In most chronic stress paradigms applicable to rodents (e.g.: restraint, foot shocks, chronic unpredictable stresses, social defeat), allostatic load is inherently coupled to sensory experiences. While it may seem intuitive that these encounters would lead to sensory maladaptation, evidence for such phenomena is scarce. Immobilization and unpredictable mild stress repeated for 1–2 weeks induced synaptic remodeling (predominantly synapse loss) and altered excitatory-inhibitory balance in the rodent somatosensory cortex (Chen et al., 2018). This study reported synapse elimination from the visual cortex as well but did not explore the visual system any further. Notably, mice in the Chen et al. study were exposed to stress starting at 1 month of age,

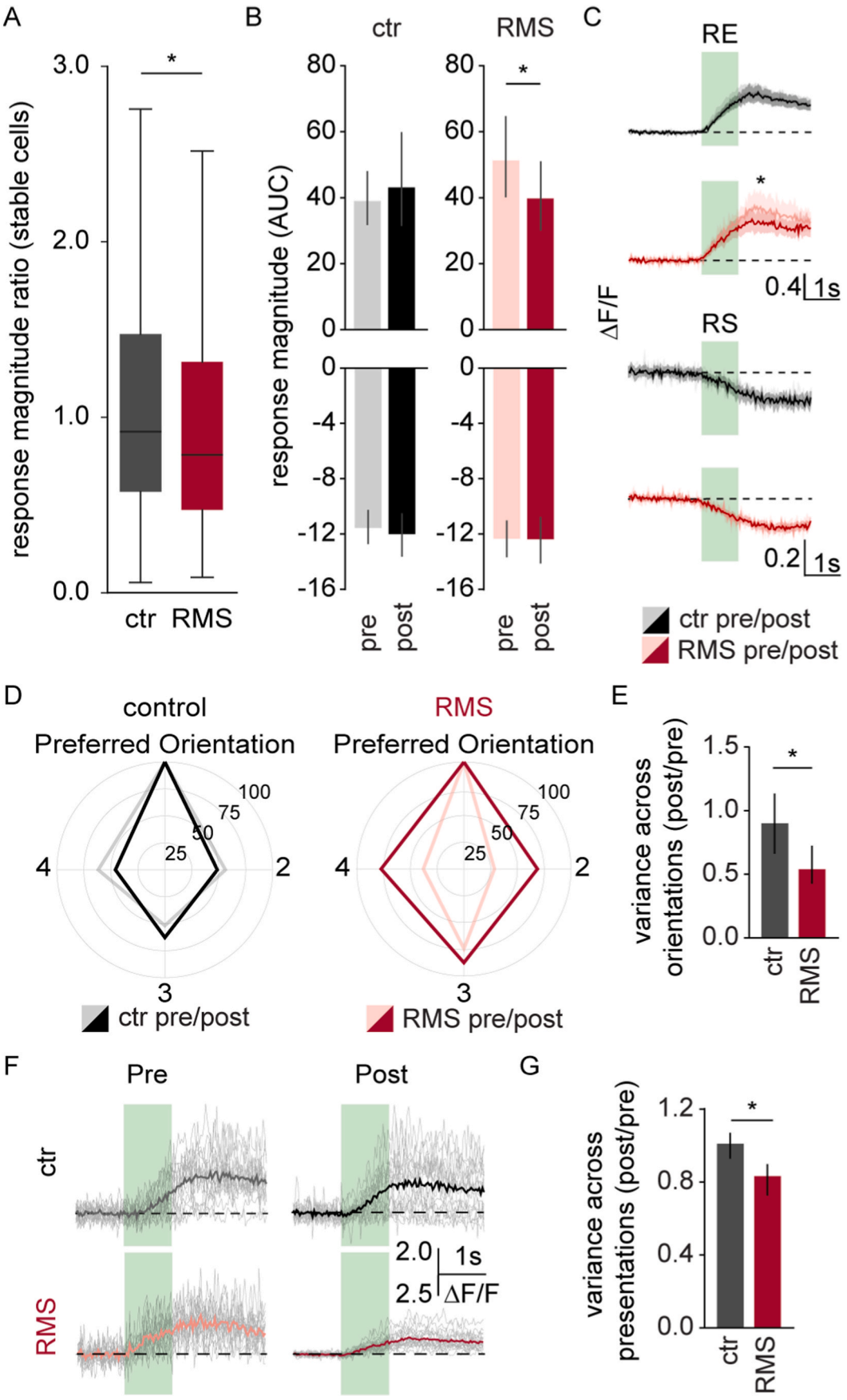

(caption on next page)

Fig. 2. RMS altered visual response characteristics in the adult PPC. (**A**) Box plot (IQR) of response magnitude ratio (post-/pre-treatment session) across all stable cells in control (grey) and RMS (red) mice. (**B**) Response magnitudes of enhanced (top) and suppressed (bottom) stable cells before (light) and after (dark) rest (black) or RMS (red). (**C**) Mean fluorescence intensity traces (solid lines) ± 95% CI (shaded areas) of enhanced (top) and suppressed (bottom) stable cells in control (black) and RMS (red) mice. Stimulus indicated by green box, scale bar shows ΔF/F. (**D**) Example polar plots showing pre- (light) and post- (dark) treatment response magnitudes normalized to the preferred orientation of cells from control (left) and RMS (right) mice. (**E**) Median change in variance (post/pre) across orientations in control (grey) and RMS (red) cells. (**F**) Example responses to the preferred orientation of a cell from control (top row) or RMS (bottom row) exposed mice before (left) or after (right) treatment. Thin lines represent individual stimulus presentations, thick lines show mean response. (**G**) Median change in variance (post/pre) across stimulus presentations in control (grey) or RMS (red) mice. *: $p < 0.05$; error bars represent 95% CI. (For interpretation of the references to color in this figure legend, the reader is referred to the Web version of this article.)

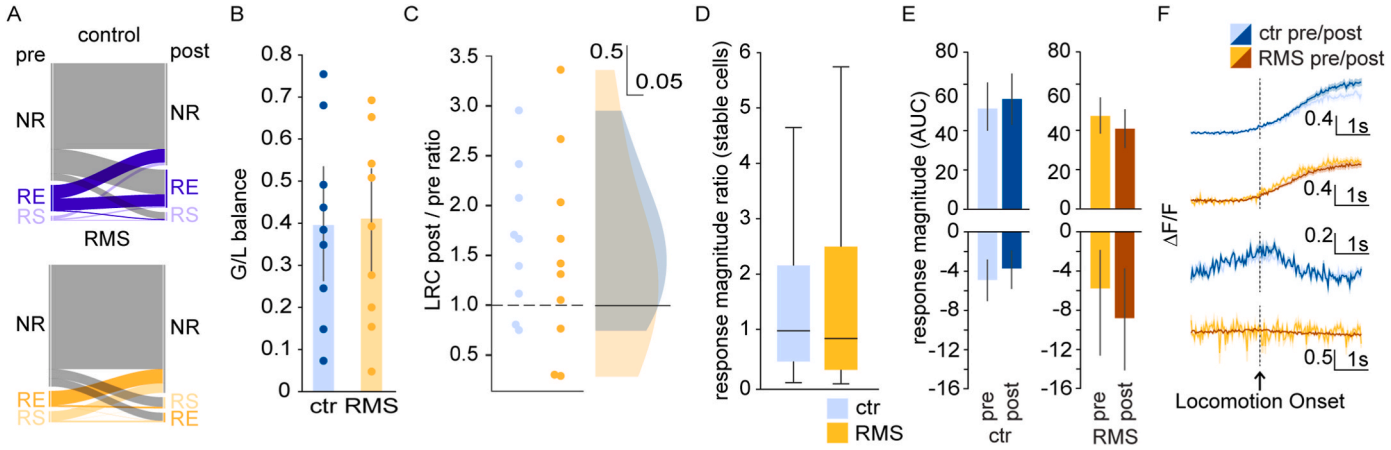

Fig. 3. RMS did not affect locomotion responses in the PPC. (**A**) Sankey plots showing pooled population dynamics. Line thickness represents the relative proportion of non-responsive (NR), responsive enhanced (RE), and responsive suppressed (RS) cells in the population. (**B**) Bars represent the G/L balance index in control (blue) and RMS (orange) mice. (**C**) Ratio of locomotion-responsive cells (LRC) before and after treatment (left) in control (blue) and RMS (orange) mice plotted next to kernel density estimate (right). (**D**) Box plot (IQR) of response magnitude ratio (post/pre) of stable cells in control (blue) and RMS (orange) mice. (**E**) Comparison of pre (light color) and post (darker color) mean locomotion response magnitudes of enhanced (top) and suppressed (bottom) stable cells in control (blues) and RMS (orange/brown) mice. (**F**) Average fluorescence intensity traces (solid lines) ± 95% CI (shaded areas) of enhanced (top) and suppressed (bottom) stable cells in control (blue) and RMS (orange) mice. Scale bar shows ΔF/F. Locomotion onset indicated by black vertical line. (For interpretation of the references to color in this figure legend, the reader is referred to the Web version of this article.)

aligning the results better to our previous work in adolescent mice (Libovner et al., 2020; Fariborzi et al., 2021). In the visual cortex, stress exposure led to reduced homogeneity measures (Li et al., 2018), or atrophy (Yoshii et al., 2017), while prolonged food restriction increased plasticity (Spolidoro et al., 2011). Our results indicate that stress exposure can have a marked impact on responsiveness in higher order sensory regions.

A critical aspect of the data presented here was that the effect of RMS on sensory responsiveness appeared highly variable across individual subjects. Similar idiosyncrasy was described in how chronic social defeat and maternal deprivation altered responses across the somatosensory cortex (McGirr et al., 2020). This study indicated that the identity of spontaneous sensory motifs affected by stress was unique to each animal. At the level of cellular responses, the authors described a substantial increase in the variance of sensory evoked responses (McGirr et al., 2020) while others found increased variance in spontaneous activity of frontal cortical neurons (Barthas et al., 2020). Indeed, which side of the bimodal distribution a mouse fell in our experiments depended on whether sensory responses were increased or decreased following stress exposure. Conversely, we found that responses to the preferred orientation of a neuron became less variable following RMS. Individual differences in stress response were noted in human subjects half a century ago (Goldstein, 1973; Sapolsky, 1994) and confirmed in a variety of species since (Carere et al., 2010). Mechanistic explorations of this variability focused on corticolimbic structures like the hippocampus, medial prefrontal cortex, bed nucleus of the stria terminalis, or the lateral septum (Ebner and Singewald, 2017), leaving questions regarding the causes of idiosyncratic responses across individual animals in sensory systems open for future studies.

Given the bimodal distribution of the population responses, grand averages offered no insight into the effect of RMS on sensory response amplitudes. Instead, we turned to cells that showed stable visually evoked responses in both imaging sessions. Separating neurons with enhanced (positive deflection) from suppressed (negative deflection) responses revealed that the change in absolute response magnitudes was exclusively driven by reduced response magnitudes in enhanced cells. Since generating a suppressed response should include a feed forward inhibitory circuit (Markram et al., 2004; Suzuki et al., 2022; Schroeder et al., 2023), the above observation suggest that excitatory inputs to pyramidal neurons were predominantly affected by RMS. The apparent lack of synapse loss in our histology experiments could be indicative of alternative mechanisms causing reduced excitatory drive in the adult PPC. Possibilities include stress-induced changes in glutamatergic transmission (Groc et al., 2008; Yuen et al., 2012; Nawreen et al., 2021) or decreased excitability of pyramidal neurons (Matovic et al., 2020; Nawreen et al., 2021). Alternatively, general PSD95 immunostaining may simply lack the sensitivity necessary to detect loss of input to a specific population of neurons. Indeed, our noise correlation measures indicate that reduced common input is at least part of the underlying mechanism (Aertsen et al., 1989; Schneidman et al., 2006; Cohen and Kohn, 2011; Panzeri et al., 2022). Future studies employing cell-type specific tracing of inputs, or optogenetic stimulation combined with electrophysiology could determine how adult RMS exposure affects the excitability and connectivity of visually responsive PPC neurons. In addition, we found a general broadening of orientation tuning in RMS exposed mice, although the proper assessment of visual tuning properties would require a more sophisticated approach (e.g. testing more than 4 orientations) than what we applied here.

Surprisingly, we found that all the above discussed effects of RMS were limited to visual processing in the parietal cortex, without any

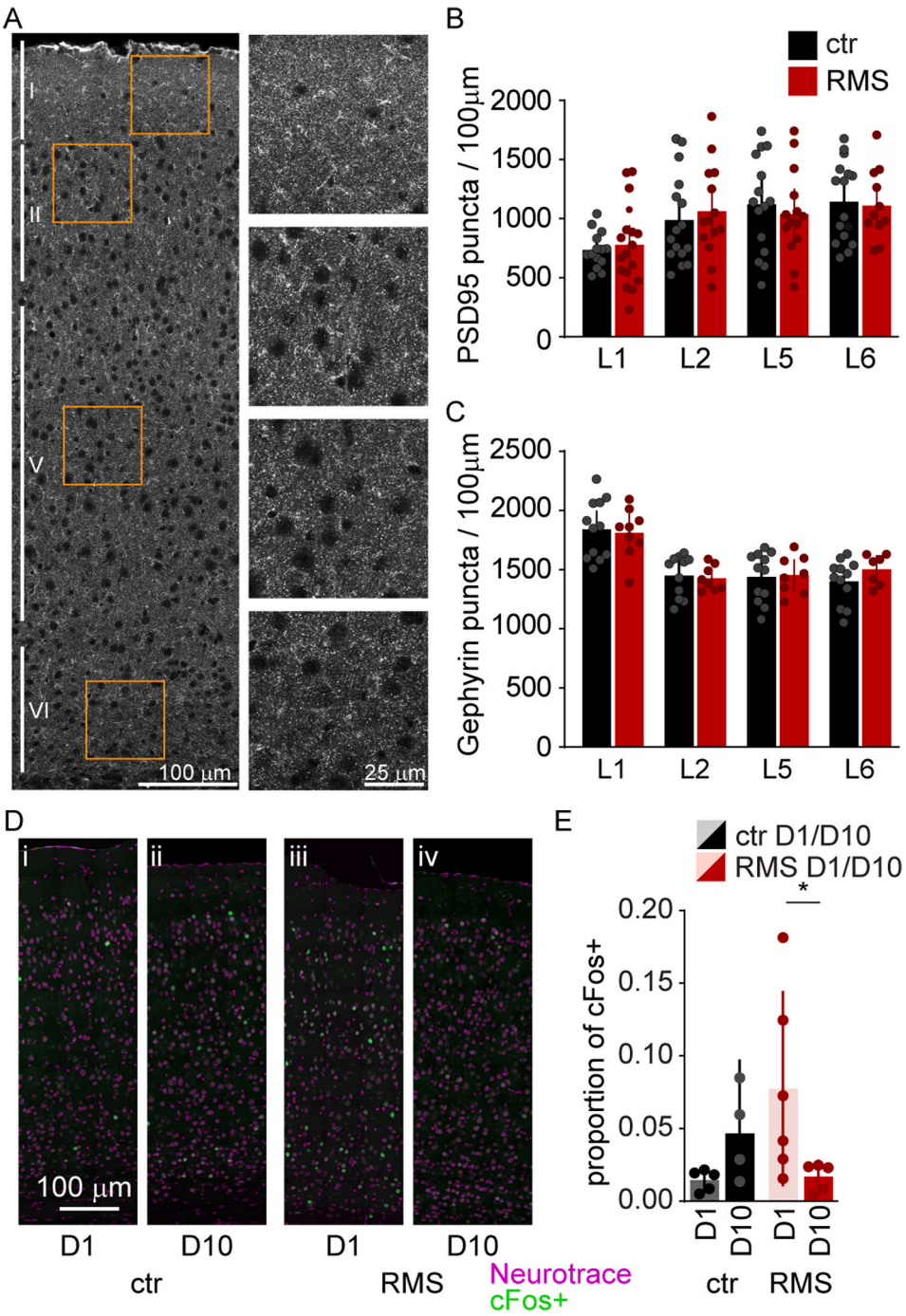

Fig. 4. RMS exposure did not affect synaptic densities in the adult PPC. (**A**) Example confocal image of a parietal cortical column (left), with excised 100 μm^2 squares used for quantifying puncta densities (right). (**B**) Quantification of PSD95 puncta density in each layer of the PPC. (**C**) Quantification of Gephyrin puncta density in each layer of the PPC. (**D**) Representative confocal images of cFos (green) and NeuroTrace (magenta) staining at Day1 (D1) and Day10 (D10) in control and RMS mice. (**E**) Quantification of the proportion of neurons expressing cFos. *: $p < 0.05$. Error bars represent 95% CI. (For interpretation of the references to color in this figure legend, the reader is referred to the Web version of this article.)

notable changes in neuronal activity related to locomotion onset. Today it is well-established that motor movements modulate neuronal activity even outside of specific motor regions (Niell and Stryker, 2010; Vinck et al., 2015). An example of this is the effect of locomotion on sensory processing (Niell and Stryker, 2010; Saleem et al., 2013; Vinck et al., 2015; Dadarlat and Stryker, 2017). Given the established role of stress-adjacent neurotransmitters (e.g. acetyl-choline and norepinephrine) in state transitions associated with locomotion (Polack et al., 2013; Fu et al., 2014; Collins et al., 2023), it was unexpected to see no RMS induced changes in neural activity associated with locomotion onset. Cholinergic and adrenergic systems are known to be affected by a variety of stress paradigms (Roth et al., 1982; Mark et al., 1996; Tajima et al., 1996; Mineur et al., 2013). The lack of effect observed here may be explained by the specifics of the RMS paradigm employed here, by the above discussed habituation effect, or by the specific region studied. Future work will need to disambiguate these possibilities to better understand why RMS exposure specifically impacted sensory processing in the parietal cortex.

We also did not find a discernible effect of RMS on the density of excitatory or inhibitory synapses using indirect immunostaining,

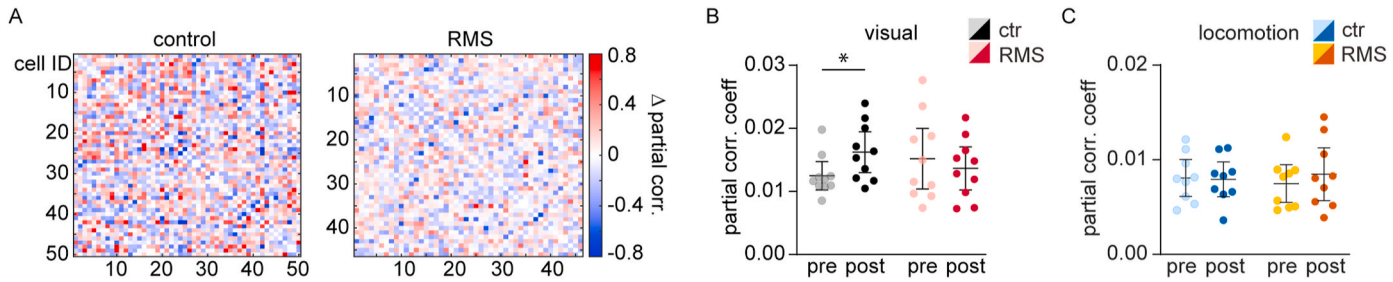

Fig. 5. RMS altered noise correlations in the PPC. (**A**) Heatmap of the change in partial correlations (post - pre treatment session) in control (left) and RMS (right) mice. (**B**) Population data of partial correlation coefficients of visually evoked responses in the first, pre- (light) and second, post- (dark) treatment session in control (black) and RMS (red) mice. (**C**) Population data of partial correlation coefficients of locomotion evoked responses in pre (light) and post (dark) treatment session in control (blue) and RMS (orange) mice. *: $p < 0.05$. Error bars represent 95% CI. (For interpretation of the references to color in this figure legend, the reader is referred to the Web version of this article.)

suggesting that en masse synapse loss does not explain RMS-induced changes in visual responsiveness in the PPC. This result is in stark contrast to our previous work, where we found evidence of significant, layer specific erosion of synaptic connectivity in the PPC following RMS exposure during adolescence (Libovner et al., 2020; Fariborzi et al., 2021). Work by other groups also indicate that stress affects the brain in an age-dependent manner (Bingham et al., 2011; Mancini et al., 2021). The mature, adult circuitry may be more robust against stress-induced remodeling of synaptic connections in part due to the ability to habituate to repeated exposure to stressors. Such attenuation was noted across a multitude of chronic stress paradigms, including restraint (Girotti et al., 2006; Grissom et al., 2007; Gray et al., 2010; Duarte et al., 2015; Matovic et al., 2019), social defeat stress (Snyder et al., 2015), and audiogenic stress (Armario et al., 1984; Campeau et al., 2002). Regularity of exposure and stress intensity are thought to be the key factors determining the activation of the HPA-axis in chronically stressed animals (Martf and Armario, 1997; Grissom and Bhatnagar, 2009). Indeed, similarly to others, we found that the first stress exposure drastically increased cFos expression in the PPC, but the number of c-Fos positive neurons diminished to control levels by the 10th day of RMS (Campeau et al., 2002; Girotti et al., 2006). This was not the case when adolescent mice were exposed to the same stress paradigm (Libovner et al., 2020). Our findings in the parietal cortex may also be in contrast to results from the hippocampus, where a single exposure to a similar stress paradigm caused marked loss of excitatory synapses (Chen et al., 2008; Maras et al., 2014; Hokenson et al., 2021). However, the effect of repeated exposure to this specific paradigm, and the possibility of habituation, in the adult hippocampus is yet to be tested. These discrepancies underscore the previously noted potential for region specific effects of stress (Meller et al., 2003; Moench et al., 2019).

CRediT authorship contribution statement

Soo Bin Park: Writing – original draft, Visualization, Investigation, Formal analysis, Data curation. **Gyorgy Lur:** Writing – review & editing, Supervision, Funding acquisition, Formal analysis, Conceptualization.

Declaration of competing interest

The authors declare that they have no known competing financial interests or personal relationships that could have appeared to influence the work reported in this paper.

Data availability

Data will be made available on request.

Acknowledgements

This work was funded by the NIMH: R01MH123686 (GL) and the NIDCD: T32DC010775-14 (SBP). We thank the Optical Biology Core Facility of the Developmental Biology Center, a shared resource supported by the Cancer Center Support Grant (CA-62203) and Center for Complex Biological Systems Support Grant (GM-076516) at the University of California, Irvine.

Appendix A. Supplementary data

Supplementary data to this article can be found online at https://doi.org/10.1016/j.ynstr.2024.100660.

References

Aertsen, A.M., Gerstein, G.L., Habib, M.K., Palm, G., 1989. Dynamics of neuronal firing correlation: modulation of "effective connectivity.". J. Neurophysiol. 61, 900–917.
Anderson, R.M., Glanz, R.M., Johnson, S.B., Miller, M.M., Romig-Martin, S.A., Radley, J. J., 2016. Prolonged corticosterone exposure induces dendritic spine remodeling and attrition in the rat medial prefrontal cortex. J. Comp. Neurol. 524, 3729–3746.
Armario, A., Castellanos, J.M., Balasch, J., 1984. Adaptation of anterior pituitary hormones to chronic noise stress in male rats. Behav. Neural. Biol. 41, 71–76.
Barthas, F., Hu, M.Y., Siniscalchi, M.J., Ali, F., Mineur, Y.S., Picciotto, M.R., Kwan, A.C., 2020. Cumulative effects of social stress on reward-guided actions and prefrontal cortical activity. Biol. Psychiatr. 88, 541–553.
Bingham, B., McFadden, K., Zhang, X., Bhatnagar, S., Beck, S., Valentino, R., 2011. Early adolescence as a critical window during which social stress distinctly alters behavior and brain norepinephrine activity. Neuropsychopharmacology 36, 896–909.
Bondi, C.O., Rodriguez, G., Gould, G.G., Frazer, A., Morilak, D.A., 2008. Chronic unpredictable stress induces a cognitive deficit and anxiety-like behavior in rats that is prevented by chronic antidepressant drug treatment. Neuropsychopharmacology 33, 320–331.
Bremner, J.D., Staib, L.H., Kaloupek, D., Southwick, S.M., Soufer, R., Charney, D.S., 1999. Neural correlates of exposure to traumatic pictures and sound in Vietnam combat veterans with and without posttraumatic stress disorder: a positron emission tomography study. Biol. Psychiatr. 45, 806–816.
Buschman, T.J., Miller, E.K., 2007. Top-down versus bottom-up control of attention in the prefrontal and posterior parietal cortices. Science 315, 1860–1862.
Campeau, S., Dolan, D., Akil, H., Watson, S.J., 2002. c-fos mRNA induction in acute and chronic audiogenic stress: possible role of the orbitofrontal cortex in habituation. Stress 5, 121–130.
Carere, C., Caramaschi, D., Fawcett, T.W., 2010. Covariation between personalities and individual differences in coping with stress: converging evidence and hypotheses. Current Zoology 56, 728–740.
Chen, C.-C., Lu, J., Yang, R., Ding, J.B., Zuo, Y., 2018. Selective activation of parvalbumin interneurons prevents stress-induced synapse loss and perceptual defects. Mol. Psychiatr. 23, 1614–1625.
Chen, Y., Dubé, C.M., Rice, C.J., Baram, T.Z., 2008. Rapid loss of dendritic spines after stress involves derangement of spine dynamics by corticotropin-releasing hormone. J. Neurosci. 28, 2903–2911.
Chen, Y., Rex, C.S., Rice, C.J., Dube, C.M., Gall, C.M., Lynch, G., Baram, T.Z., 2010. Correlated memory defects and hippocampal dendritic spine loss after acute stress involve corticotropin-releasing hormone signaling. Proc. Natl. Acad. Sci. U. S. A. 107, 13123–13128.
Cohen, M.R., Kohn, A., 2011. Measuring and interpreting neuronal correlations. Nat. Neurosci. 14, 811–819.
Collins, L., Francis, J., Emanuel, B., McCormick, D.A., 2023. Cholinergic and noradrenergic axonal activity contains a behavioral-state signal that is coordinated

across the dorsal cortex Nelson SB. In: Huguenard, J.R., London, M. (Eds.), Elife 12, e81826.
Dadarlat, M.C., Stryker, M.P., 2017. Locomotion enhances neural encoding of visual stimuli in mouse V1. J. Neurosci. 37, 3764–3775.
de Kloet, E.R., Joëls, M., Holsboer, F., 2005. Stress and the brain: from adaptation to disease. Nat. Rev. Neurosci. 6, 463–475.
Duarte, J.O., Cruz, F.C., Leão, R.M., Planeta, C.S., Crestani, C.C., 2015. Stress vulnerability during adolescence: comparison of chronic stressors in adolescent and adult rats. Psychosom. Med. 77, 186.
Ebner, K., Singewald, N., 2017. Individual differences in stress susceptibility and stress inhibitory mechanisms. Current Opinion in Behavioral Sciences 14, 54–64.
Eckart, C., Stoppel, C., Kaufmann, J., Tempelmann, C., Hinrichs, H., Elbert, T., Heinze, H.-J., Kolassa, I.-T., 2011. Structural alterations in lateral prefrontal, parietal and posterior midline regions of men with chronic posttraumatic stress disorder. J. Psychiatry Neurosci. 36, 176–186.
Fariborzi, M., Park, S.B., Ozgur, A., Lur, G., 2021. Sex-dependent long-term effects of prepubescent stress on the posterior parietal cortex. Neurobiology of Stress 14, 100295.
Fu, Y., Tucciarone, J.M., Espinosa, J.S., Sheng, N., Darcy, D.P., Nicoll, R.A., Huang, Z.J., Stryker, M.P., 2014. A cortical circuit for gain control by behavioral state. Cell 156, 1139–1152.
Girotti, M., Pace, T.W.W., Gaylord, R.I., Rubin, B.A., Herman, J.P., Spencer, R.L., 2006. Habituation to repeated restraint stress is associated with lack of stress-induced c-fos expression in primary sensory processing areas of the rat brain. Neuroscience 138, 1067–1081.
Goldstein, M.J., 1973. Individual differences in response to stress. Am. J. Community Psychol. 1, 113–137.
Gray, M., Bingham, B., Viau, V., 2010. A comparison of two repeated restraint stress paradigms on hypothalamic-pituitary-adrenal axis habituation, gonadal status and central neuropeptide expression in adult male rats. J. Neuroendocrinol. 22, 92–101.
Grissom, N., Bhatnagar, S., 2009. Habituation to repeated stress: get used to it. Neurobiol. Learn. Mem. 92, 215–224.
Grissom, N., Iyer, V., Vining, C., Bhatnagar, S., 2007. The physical context of previous stress exposure modifies hypothalamic–pituitary–adrenal responses to a subsequent homotypic stress. Horm. Behav. 51, 95–103.
Groc, L., Choquet, D., Chaouloff, F., 2008. The stress hormone corticosterone conditions AMPAR surface trafficking and synaptic potentiation. Nat. Neurosci. 11, 868–870.
Hartigan, J.A., Hartigan, P.M., 1985. The dip test of unimodality. Ann. Stat. 13 (1), 70–84. http://www.jstor.org/stable/2241144.
Hokenson, R.E., Oijala, M., Short, A.K., Bolton, J.L., Chen, Y., Molet, J., Maras, P.M., Baram, T.Z., Lur, G., 2020. Multiple simultaneous acute stresses in mice: single or repeated induction. Bio Protoc 10, e3699.
Hokenson, R.E., Short, A.K., Chen, Y., Pham, A.L., Adams, E.T., Bolton, J.L., Swarup, V., Gall, C.M., Baram, T.Z., 2021. Unexpected role of physiological estrogen in acute stress-induced memory deficits. J. Neurosci. 41, 648–662.
Jeanneteau, F., Barrère, C., Vos, M., De Vries, C.J.M., Rouillard, C., Levesque, D., Dromard, Y., Moisan, M.-P., Duric, V., Franklin, T.C., Duman, R.S., Lewis, D.A., Ginsberg, S.D., Arango-Lievano, M., 2018. The stress-induced transcription factor NR4A1 adjusts mitochondrial function and synapse number in prefrontal cortex. J. Neurosci. 38, 1335–1350.
Knauft, K., Waldron, A., Mathur, M., Kalia, V., 2021. Perceived chronic stress influences the effect of acute stress on cognitive flexibility. Sci. Rep. 11, 23629.
Lamprecht, M.R., Sabatini, D.M., Carpenter, A.E., 2007. CellProfiler™: free, versatile software for automated biological image analysis. Biotechniques 42, 71–75.
Li, J., Yang, R., Xia, K., Wang, T., Nie, B., Gao, K., Chen, J., Zhao, H., Li, Y., Wang, W., 2018. Effects of stress on behavior and resting-state fMRI in rats and evaluation of Telmisartan therapy in a stress-induced depression model. BMC Psychiatr. 18, 337.
Libovner, Y., Fariborzi, M., Tabba, D., Ozgur, A., Jafar, T., Lur, G., 2020. Repeated exposure to multiple concurrent stresses induce circuit specific loss of inputs to the posterior parietal cortex. J. Neurosci. 40, 1849–1861.
Liston, C., McEwen, B.S., Casey, B.J., 2009. Psychosocial stress reversibly disrupts prefrontal processing and attentional control. Proc. Natl. Acad. Sci. U. S. A. 106, 912–917.
Lkhagvasuren, B., Oka, T., Nakamura, Y., Hayashi, H., Sudo, N., Nakamura, K., 2014. Distribution of Fos-immunoreactive cells in rat forebrain and midbrain following social defeat stress and diazepam treatment. Neuroscience 272, 34–57.
Lur, G., Vinck, M.A., Tang, L., Cardin, J.A., Higley, M.J., 2016. Projection-specific visual feature encoding by layer 5 cortical subnetworks. Cell Rep. 14, 2538–2545.
Mancini, G.F., Marchetta, E., Riccardi, E., Trezza, V., Morena, M., Campolongo, P., 2021. Sex-divergent long-term effects of single prolonged stress in adult rats. Behav. Brain Res. 401, 113096.
Maras, P.M., Molet, J., Chen, Y., Rice, C., Ji, S.G., Solodkin, A., Baram, T.Z., 2014. Preferential loss of dorsal-hippocampus synapses underlies memory impairments provoked by short, multimodal stress. Mol. Psychiatr. 19, 811–822.
Mark, G.P., Rada, P.V., Shors, T.J., 1996. Inescapable stress enhances extracellular acetylcholine in the rat hippocampus and prefrontal cortex but not the nucleus accumbens or amygdala. Neuroscience 74, 767–774.
Markram, H., Toledo-Rodriguez, M., Wang, Y., Gupta, A., Silberberg, G., Wu, C., 2004. Interneurons of the neocortical inhibitory system. Nat. Rev. Neurosci. 5, 793–807.
Martf, O., Armario, A., 1997. Influence of regularity of exposure to chronic stress on the pattern of habituation of pituitary-adrenal hormones, prolactin and glucose. Stress 1, 179–189.
Matovic, S., Ichiyama, A., Igarashi, H., Salter, E.W., Sunstrum, J.K., Wang, X.F., Henry, M., Kuebler, E.S., Vernoux, N., Martinez-Trujillo, J., Tremblay, M., Inoue, W., 2020. Neuronal hypertrophy dampens neuronal intrinsic excitability and stress responsiveness during chronic stress. J. Physiol. 598, 2757–2773.
Matovic, S., Ichiyama, A., Igarashi, H., Salter, E.W., Wang, X.-F., Henry, M., Vernoux, N., Tremblay, M.-E., Inoue, W., 2019. Stress-induced neuronal hypertrophy decreases the intrinsic excitability in stress habituation. Available at: https://www.biorxiv.org/content/10.1101/593665v1. (Accessed 17 October 2023).
McGirr, A., LeDue, J., Chan, A.W., Boyd, J.D., Metzak, P.D., Murphy, T.H., 2020. Stress impacts sensory variability through cortical sensory activity motifs. Transl. Psychiatry 10, 20.
Meller, E., Shen, C., Nikolao, T.A., Jensen, C., Tsimberg, Y., Chen, J., Gruen, R.J., 2003. Region-specific effects of acute and repeated restraint stress on the phosphorylation of mitogen-activated protein kinases. Brain Res. 979, 57–64.
Mineur, Y.S., Obayemi, A., Wigestrand, M.B., Fote, G.M., Calarco, C.A., Li, A.M., Picciotto, M.R., 2013. Cholinergic signaling in the hippocampus regulates social stress resilience and anxiety- and depression-like behavior. Proc. Natl. Acad. Sci. USA 110, 3573–3578.
Mitra, R., Jadhav, S., McEwen, B.S., Vyas, A., Chattarji, S., 2005. Stress duration modulates the spatiotemporal patterns of spine formation in the basolateral amygdala. Proc. Natl. Acad. Sci. U. S. A. 102, 9371–9376.
Moench, K.M., Breach, M.R., Wellman, C.L., 2019. Chronic stress produces enduring sex- and region-specific alterations in novel stress-induced c-Fos expression. Neurobiology of Stress 10, 100147.
Nawreen, N., Baccei, M.L., Herman, J.P., 2021. Single prolonged stress reduces intrinsic excitability and excitatory synaptic drive onto pyramidal neurons in the infralimbic prefrontal cortex of adult male rats. Front. Cell. Neurosci. 15. Available at: https://www.frontiersin.org/articles/10.3389/fncel.2021.705660. (Accessed 22 January 2024).
Niell, C.M., Stryker, M.P., 2010. Modulation of visual responses by behavioral state in mouse visual cortex. Neuron 65, 472–479.
Ozgur, A., Park, S.B., Flores, A.Y., Oijala, M., Lur, G., 2023. A comprehensive, affordable, open-source hardware-software solution for flexible implementation of Complex behaviors in head-fixed mice. eNeuro 10:ENEURO 18, 23.2023.
Pachitariu, M., Stringer, C., Dipoppa, M., Schröder, S., Rossi, L.F., Dalgleish, H., Carandini, M., Harris, K.D., 2016. Suite2p: beyond 10,000 neurons with standard two-photon microscopy. Neuroscience. Available at: http://biorxiv.org/lookup/doi/10.1101/061507. (Accessed 20 October 2023).
Panzeri, S., Moroni, M., Safaai, H., Harvey, C.D., 2022. The structures and functions of correlations in neural population codes. Nat. Rev. Neurosci. 23, 551–567.
Polack, P.-O., Friedman, J., Golshani, P., 2013. Cellular mechanisms of brain state–dependent gain modulation in visual cortex. Nat. Neurosci. 16, 1331–1339.
Radley, J.J., Anderson, R.M., Hamilton, B.A., Alcock, J.A., Romig-Martin, S.A., 2013. Chronic stress-induced alterations of dendritic spine subtypes predict functional decrements in an hypothalamo-pituitary-adrenal-inhibitory prefrontal circuit. J. Neurosci. 33, 14379–14391.
Radley, J.J., Rocher, A.B., Miller, M., Janssen, W.G.M., Liston, C., Hof, P.R., McEwen, B.S., Morrison, J.H., 2006. Repeated stress induces dendritic spine loss in the rat medial prefrontal cortex. Cerebr. Cortex 16, 313–320.
Rodrigues, D., Monteiro, P., 2023. Chronic stress promotes basal ganglia disinhibition by increasing the excitatory drive of direct-pathway neurons. Neurobiology of Stress 27, 100571.
Roth, K.A., Mefford, I.M., Barchas, J.D., 1982. Epinephrine, norepinephrine, dopamine and serotonin: differential effects of acute and chronic stress on regional brain amines. Brain Res. 239, 417–424.
Saleem, A.B., Ayaz, A., Jeffery, K., Harris, K.D., Carandini, M., 2013. Integration of visual motion and locomotion in mouse visual cortex. Nat. Neurosci. 16, 1864–1869.
Sapolsky, R.M., 1994. Individual differences in the stress response. Semin. Neurosci. 6, 261–269.
Schneidman, E., Berry, M.J., Segev, R., Bialek, W., 2006. Weak pairwise correlations imply strongly correlated network states in a neural population. Nature 440, 1007–1012.
Schroeder, A., Pardi, M.B., Keijser, J., Dalmay, T., Groisman, A.I., Schuman, E.M., Sprekeler, H., Letzkus, J.J., 2023. Inhibitory top-down projections from zona incerta mediate neocortical memory. Neuron 111, 727–738.e8.
Shackman, A.J., Salomons, T.V., Slagter, H.A., Fox, A.S., Winter, J.J., Davidson, R.J., 2011. The integration of negative affect, pain and cognitive control in the cingulate cortex. Nat. Rev. Neurosci. 12, 154–167.
Snyder, K.P., Barry, M., Valentino, R.J., 2015. Cognitive impact of social stress and coping strategy throughout development. Psychopharmacology 232, 185–195.
Sousa, N., Almeida, O.F.X., 2012. Disconnection and reconnection: the morphological basis of (mal)adaptation to stress. Trends Neurosci. 35, 742–751.
Spolidoro, M., Baroncelli, L., Putignano, E., Maya-Vetencourt, J.F., Viegi, A., Maffei, L., 2011. Food restriction enhances visual cortex plasticity in adulthood. Nat. Commun. 2, 320.
Spooner, R.K., Taylor, B.K., L'Heureux, E., Schantell, M., Arif, Y., May, P.E., Morsey, B., Wang, T., Ideker, T., Fox, H.S., Wilson, T.W., 2021. Stress-induced aberrations in sensory processing predict worse cognitive outcomes in healthy aging adults. Aging (Albany NY) 13, 19996–20015.
Suzuki, A., Kosugi, S., Murayama, E., Sasakawa, E., Ohkawa, N., Konno, A., Hirai, H., Inokuchi, K., 2022. A cortical cell ensemble in the posterior parietal cortex controls past experience-dependent memory updating. Nat. Commun. 13, 41.
Tajima, T., Endo, H., Suzuki, Y., Ikari, H., Gotoh, M., Iguchi, A., 1996. Immobilization stress-induced increase of hippocampal acetylcholine and of plasma epinephrine, norepinephrine and glucose in rats. Brain Res. 720, 155–158.
Vinck, M., Batista-Brito, R., Knoblich, U., Cardin, J.A., 2015. Arousal and locomotion make distinct contributions to cortical activity patterns and visual encoding. Neuron 86, 740–754.

Vyas, A., Mitra, R., Shankaranarayana Rao, B.S., Chattarji, S., 2002. Chronic stress induces contrasting patterns of dendritic remodeling in hippocampal and amygdaloid neurons. J. Neurosci. 22, 6810–6818.
Whitlock, J.R., 2017. Posterior parietal cortex. Curr. Biol. 27, R691–R695.
Woolley, C.S., Gould, E., McEwen, B.S., 1990. Exposure to excess glucocorticoids alters dendritic morphology of adult hippocampal pyramidal neurons. Brain Res. 531, 225–231.
Yochman, A., Pat-Horenczyk, R., 2020. Sensory modulation in children exposed to continuous traumatic stress. J. Child Adolesc. Trauma 13, 93–102.
Yoshii, T., Oishi, N., Ikoma, K., Nishimura, I., Sakai, Y., Matsuda, K., Yamada, S., Tanaka, M., Kawata, M., Narumoto, J., Fukui, K., 2017. Brain atrophy in the visual cortex and thalamus induced by severe stress in animal model. Sci. Rep. 7, 12731.
Yuen, E.Y., Wei, J., Liu, W., Zhong, P., Li, X., Yan, Z., 2012. Repeated stress causes cognitive impairment by suppressing glutamate receptor expression and function in prefrontal cortex. Neuron 73, 962–977.
Zhang, H.-H., Meng, S.-Q., Guo, X.-Y., Zhang, J.-L., Zhang, W., Chen, Y.-Y., Lu, L., Yang, J.-L., Xue, Y.-X., 2019. Traumatic stress produces delayed alterations of synaptic plasticity in basolateral amygdala. Front. Psychol. 10, 2394.
Zhou, Y., Freedman, D.J., 2019. Posterior parietal cortex plays a causal role in perceptual and categorical decisions. Science 365, 180–185.